



## Abstract

The extending archive of the Greenhouse Gases Observing SATellite (GOSAT) measurements (now covering about six years) allows increasingly robust statistics to be computed, that document the performance of the corresponding retrievals of the column-average dry air-mole fraction of  $\text{CO}_2$  ( $\text{XCO}_2$ ). Here, we demonstrate that atmospheric inversions cannot be rigorously optimal when assimilating current  $\text{XCO}_2$  retrievals, even with averaging kernels, in particular because retrievals and inversions use different assumption about prior uncertainty. We look for some practical evidence of this sub-optimality from the view point of atmospheric inversion by comparing a model simulation constrained by surface air-sample measurements with one of the GOSAT retrieval products (NASA's ACOS). The retrieval-minus-model differences result from various error sources, both in the retrievals and in the simulation: we discuss the plausibility of the origin of the major patterns. We find systematic retrieval errors over the dark surfaces of high-latitude lands and over African savannahs. More importantly, we also find a systematic over-fit of the GOSAT radiances by the retrievals over land for the high-gain detector mode, which is the usual observation mode. The over-fit is partially compensated by the retrieval bias-correction. These issues are likely common to other retrieval products and may explain some of the surprising and inconsistent  $\text{CO}_2$  atmospheric inversion results obtained with the existing GOSAT retrieval products. We suggest that reducing the observation weight in the retrieval schemes (for instance so that retrieval increments to the retrieval prior values are halved for the studied retrieval product) would significantly improve the retrieval quality and reduce the need for (or at least reduce the complexity of) ad-hoc retrieval bias correction.

## 1. Introduction

CO<sub>2</sub> surface fluxes at the Earth's surface can be inferred from accurate surface measurements of CO<sub>2</sub> concentrations, but the sparseness of the current global network still leaves the flux horizontal and temporal gradients, and even their latitudinal distribution, very uncertain (Peylin et al. 2013). This limitation has provided a major incentive to develop the monitoring of CO<sub>2</sub> concentrations from space. First retrievals were obtained from existing instruments measuring either the thermal infrared radiation emitted by the atmosphere (Chédin et al. 2003) or the reflected sunlight in the near-infrared (NIR)/ shortwave infrared (SWIR) spectral regions (Buchwitz et al. 2005). The latter technique allows retrieving XCO<sub>2</sub> while the former is not sensitive to CO<sub>2</sub> in the lower atmosphere, near the CO<sub>2</sub> sources and sinks. Since active (lidar) measurement techniques for XCO<sub>2</sub> from space are still in development (e.g., Ingmann et al. 2009), NIR/SWIR measurements currently offer the best prospect to provide “retrievals of CO<sub>2</sub> of sufficient quality to estimate regional sources and sinks”, as phrased by objective A.8.1 of the Global Climate Observing System programme (GCOS, 2010), in the short term. However, they are hampered by uncertain knowledge about scatterers in the atmosphere at the corresponding wavelengths (aerosols and cirrus clouds) with an effect that varies with surface albedo, which is itself uncertain (e.g., Aben et al. 2007). Such interference in the XCO<sub>2</sub> signal seen in the NIR/SWIR measurements is of concern because even sub-ppm systematic errors (corresponding to less than 0.25% of the signal) can severely flaw the inversion of CO<sub>2</sub> surface fluxes (Chevallier et al. 2007, Miller et al. 2007). This risk motivated dedicated developments of the retrieval algorithms in order to de-convolve the spectral signatures of the involved compounds as much as possible (e.g., Reuter et al. 2010, Guerlet et al. 2013b).

The Japanese GOSAT, launched in January 2009, and the USA second Orbiting Carbon Observatory (OCO-2), launched in July 2014, observe the NIR/SWIR radiation with unprecedented spectral resolution in order to specifically address this remote sensing challenge. The GOSAT archive already covers six years and can provide good insight into the adequacy of NIR/SWIR retrievals for CO<sub>2</sub> source-sink inversion. In terms of random errors, raw GOSAT retrievals now reach single shot precision better than 2 ppm (one sigma) in fair measurement conditions (e.g., Nguyen et al. 2014). This performance is better than what pre-launch studies suggested: for instance Maksuytov et al. (2008) expected 2.5-10 ppm single shot precision only. Systematic errors are difficult to quantify or else they would be removed. They are likely state-dependent with absolute values varying in time and space about the ppm before any bias correction (Nguyen et al. 2014). They also depend on the retrieval algorithm (e.g., Oshchepkov et al. 2013). As expected, the remaining uncertainty has profound impact on CO<sub>2</sub> source-sink inversions (Basu et al. 2013, Chevallier et al. 2014), but XCO<sub>2</sub> retrievals have already served as a basis to study the carbon budgets of some regions (Guerlet et al. 2013a, Basu et al. 2014, Reuter et al. 2014). For instance, 25 scientists analysed several XCO<sub>2</sub> retrievals over continental Europe and concluded that the current understanding of the European carbon sink brought by bottom-up inventories had to be revisited (Reuter et al. 2014).

This paper aims at contributing to the debate about the relevance of current GOSAT retrievals for atmospheric inversions. Our starting point is a critical review of the basic principles behind the current processing chains that go in successive steps from GOSAT measured radiance spectra to surface flux estimates (Section 3). We then focus on the GOSAT retrievals provided by NASA's Atmospheric CO<sub>2</sub> Observations from Space project (ACOS, build 3.4, described in Section 2) for the period between June 2009 and May 2013. They are of particular interest because they have been processed in a way that prefigures the official OCO-2 retrievals in terms

of spectral bands and available simultaneous observations (O'Dell et al. 2012). In Section 4, we analyse the residuals between the ACOS-GOSAT retrievals and the simulated CO<sub>2</sub> concentration fields of the Monitoring Atmospheric Chemistry and Climate atmospheric inversion product (MAACC, version 13r1, also described in Section 2) that assimilated surface air sample measurements from various networks. Concluding discussion follows in Section 5.

## **2. Retrievals and model simulation**

### **2.1. ACOS-GOSAT retrievals**

GOSAT is a joint venture by the Japan Aerospace Exploration Agency (JAXA), the National Institute for Environmental Studies (NIES) and the Ministry of the Environment (MOE) in Japan. This spacecraft is operated in a sun-synchronous polar orbit that crosses the Equator at about 13:00 local time during daytime and that repeats every 3 days. As described by O'Dell et al. (2012) and Osterman et al. (2013), the ACOS algorithm retrieves XCO<sub>2</sub> from a selection of GOSAT measurements of reflected sunlight made in the same spectral bands than OCO-2. Over land, such measurements are made by pointing the instrument to the Earth on both sides of the satellite track. Given the low reflectivity of water surfaces, ocean measurements are only possible when the instrument is pointed to the sun-glint spot, which is only done within 40° from the Equator in the summer hemisphere. GOSAT also carries a cloud and aerosol imager that can help filtering difficult scenes out, but unlike other GOSAT retrieval algorithms, ACOS does not use it since OCO-2 does not contain a similar instrument.

Following Boesch et al. (2006) and Connor et al. (2008), the ACOS algorithm relies on optimal estimation (i.e. Bayesian methods) to retrieve the vertical profile of the CO<sub>2</sub> dry air mole

fraction together with variables interfering in the measurements: the surface pressure and the surface albedo, some variables describing temperature, water vapour, clouds and aerosols in the atmosphere, and channel offsets for the instrument. The retrieved  $\text{XCO}_2$  is simply obtained by integrating the retrieved  $\text{CO}_2$  profile. In this Bayesian formulation of the retrieval, prior information about  $\text{CO}_2$  is given an artificially small weight in order to maximize the observation contribution to the result: for instance, the standard deviation of the uncertainty assigned to the prior  $\text{XCO}_2$  is larger than 10 ppm (O'Dell et al., 2012), i.e. larger than typical variations of  $\text{XCO}_2$  at the continental scale (e.g., Keppel-Aleks et al. 2011). We will discuss the impact of this choice later and for simplicity, we will call  $\text{XCO}_2^b$  and  $\text{XCO}_2^a$  the prior (*background*) and the retrieved (*analysed*)  $\text{XCO}_2$ , respectively.  $\text{XCO}_2^a$  can be compared with model simulations, as will be done here, or with other measurements via the associated  $\text{CO}_2$  averaging kernel profiles and prior profiles (e.g., Connor et al., 1994). For nadir viewing,  $\text{XCO}_2^a$  is representative of a volume that has a circular footprint at the Earth's surface of diameter about 10 km.

Previous comparisons between  $\text{XCO}_2^a$  and model simulations or reference ground-based  $\text{XCO}_2$  measurements from Total Carbon Column Observing Network (TCCON) highlighted some systematic dependency of the error of  $\text{XCO}_2^a$  as a function of a series of internal variables of the algorithm (Wunch et al. 2011b). This feature reveals some limitations of the algorithm but also allows correcting them empirically, for instance before they are assimilated in atmospheric inversion systems (Crisp et al. 2012). We will call  $\text{XCO}_2^{a,c}$  the bias-corrected retrievals.

## 2.2. MACC $\text{CO}_2$ inversion

Since year 2011, the MACC pre-operational service ([www.copernicus-atmosphere.eu](http://www.copernicus-atmosphere.eu)) has been delivering a  $\text{CO}_2$  inversion product with biannual updates. Release 13r1 primarily describes

the CO<sub>2</sub> surface fluxes over more than three decades, from 1979 to 2013, at resolution 3.75° × 1.9° (longitude-latitude) and 3-hourly, based on 131 CO<sub>2</sub> dry air mole fraction station records from three large databases:

- the NOAA Earth System Research Laboratory archive (NOAA CCGG, <http://www.esrl.noaa.gov/gmd/ccgg/index.html>),
- the World Data Centre for Greenhouse Gases archive (WDCGG, <http://ds.data.jma.go.jp/gmd/wdcgg/>),
- the Réseau Atmosphérique de Mesure des Composés à Effet de Serre database (RAMCES, <http://www.lsce.ipsl.fr/>).

The three databases include both in situ measurements made by automated quasi-continuous analysers and irregular air samples collected in flasks and later analyzed in central facilities. The detailed list of sites is provided in Tables 1 and 2.

The MACC Bayesian inversion method is formulated in a variational way in order to estimate the CO<sub>2</sub> surface fluxes at the above-described relatively high resolution over the globe (Chevallier et al. 2005, 2010). For v13r1, the system used a single 35-year inversion window, therefore enforcing physical and statistical consistency in the inverted fluxes. Fluxes and mole fractions are linked in the system by the global atmospheric transport model of the Laboratoire de Météorologie Dynamique (LMDZ, Hourdin et al. 2006) with 39 layers in the vertical and with the same horizontal resolution than the inverted fluxes. LMDZ is nudged to ECMWF-analysed winds for flux inversion.

The MACC inversion product also contains the 4D CO<sub>2</sub> field that is associated to the inverted surface fluxes through the LMDZ transport model. Simulating the GOSAT retrievals from this field is nearly straight-forward. The only difficulty lies in the interpolation from the LMDZ 39-level vertical grid to the 20-level vertical grid of the retrievals, before the retrieval averaging

kernels are applied. Indeed, the model orography at resolution  $3.75^\circ \times 1.9^\circ$  significantly differs from the high-resolution orography seen by the retrievals. For the interpolation, we assume that CO<sub>2</sub> concentrations vary linearly with the pressure in the vertical. When the model surface pressure is smaller than the retrieved surface pressure, the profile is artificially extended at constant value below the model surface. In the opposite case, model levels below the sounding surface are ignored. We compensate this artificial change of mass in the profile by systematically adjusting the interpolated profile so that its pressure-weighted mean equals that of the profile before the interpolation.

### 3. Theoretical aspects

Like the other retrieval and inversion systems (see, e.g., Oshchepkov et al., 2013, and Peylin et al., 2013), ACOS-GOSAT and MACC both follow the Bayesian paradigm in its Gaussian linear form (e.g., Rodgers, 2000) in order to estimate the most likely state, in a statistical sense, of the CO<sub>2</sub> profile and of the CO<sub>2</sub> surface fluxes, respectively. In mathematical terms, given  $\mathbf{x}$  the vector that gathers the variables to be inferred (either a 1D CO<sub>2</sub> profile or 2D+1D CO<sub>2</sub> surface fluxes), given  $\mathbf{x}^b$  an a priori value of  $\mathbf{x}$  (coming from a climatology or from a model), and given  $\mathbf{y}$  the vector that gathers all relevant observations (either radiances or retrievals), the most likely state of  $\mathbf{x}$  is written:

$$\mathbf{x}^a = \mathbf{x}^b + \mathbf{K}(\mathbf{y} - \mathbf{H} \mathbf{x}^b) \quad (1)$$

$\mathbf{H}$  is a linearized observation operator that links variables  $\mathbf{x}$  and  $\mathbf{y}$  (i.e. essentially a radiative transfer model or a transport model).  $\mathbf{K}$  is the following “Kalman gain” matrix:

$$\mathbf{K} = \mathbf{B} \mathbf{H}^T (\mathbf{H} \mathbf{B} \mathbf{H}^T + \mathbf{R})^{-1} \quad (2)$$

$\mathbf{B}$  and  $\mathbf{R}$  are the error covariance matrices of  $\mathbf{x}^b$  and  $\mathbf{y}$ , respectively.



The error covariance matrix of  $\mathbf{x}^a$  is obtained by:

$$\mathbf{A} = (\mathbf{I} - \mathbf{KH}) \mathbf{B} \quad (3)$$

with  $\mathbf{I}$  the identity matrix with appropriate dimension.

For simplicity, Eq. (1) does not make other variables that are simultaneously inferred appear, like clouds, aerosols or surface variables for the retrievals, or the 3D state of  $\text{CO}_2$  at the start of the assimilation window for the inversion.

The current processing chains that go from radiances to surface fluxes are two-step processes (let aside some attempts to introduce an additional intermediate step in the form of a short-window analysis of the 3D concentrations; Engelen et al. 2009). We now distinguish the retrieval process and the inversion process by putting breves  $\breve{\phantom{x}}$  on all symbols related to the former and hats  $\hat{\phantom{x}}$  on all symbols related to the latter. In a first step, the  $\text{CO}_2$  profiles and their uncertainty  $\{\breve{\mathbf{x}}^a, \breve{\mathbf{A}}\}$  are retrieved for each sounding  $\{\breve{\mathbf{y}}, \breve{\mathbf{R}}\}$  separately. The resulting ensemble forms the observations to be simultaneously assimilated  $\{\hat{\mathbf{y}}, \hat{\mathbf{R}}\}$  for the second step. The presence of prior information  $\mathbf{x}^b$  in both steps complicates the transition between the two. Following Connor et al. (1994) and the current practice, we can technically eliminate the influence of  $\mathbf{x}^b$  (but not of its uncertainty) by the following adaptation of Eq. (1) in the second step: we assimilate  $\hat{\mathbf{y}}' = \breve{\mathbf{x}}^a - (\mathbf{I} - \breve{\mathbf{K}}\breve{\mathbf{H}})\mathbf{x}^b = \breve{\mathbf{K}}\breve{\mathbf{y}}$  rather than  $\hat{\mathbf{y}}$  and change the observation operator from  $\hat{\mathbf{H}}$  to  $\hat{\mathbf{H}}' = \breve{\mathbf{K}}\breve{\mathbf{H}}\hat{\mathbf{H}}$ .  $\breve{\mathbf{K}}\breve{\mathbf{H}}$  is called the retrieval *averaging kernel*. The retrieval error covariance matrix should consistently be diminished (e.g., Connor et al., 2008, paragraph 37) and is then called  $\hat{\mathbf{R}}'$  hereafter.

For simplicity, and without loss of generality in our linear framework, let us consider the assimilation of a single sounding  $\{\breve{\mathbf{y}}, \breve{\mathbf{R}}\}$  using its averaging kernel. By definition, given the changes made to  $\hat{\mathbf{H}}$  and  $\hat{\mathbf{R}}$ , the gain matrix changes as well and we call  $\hat{\mathbf{K}}'$  the new one. By

applying Eq. (1) in this configuration, the analysed surface fluxes can be directly expressed in a concise form:

$$\hat{\mathbf{x}}^a = \hat{\mathbf{x}}^b + \hat{\mathbf{K}}' \check{\mathbf{K}} (\check{\mathbf{y}} - \check{\mathbf{H}} \hat{\mathbf{H}} \hat{\mathbf{x}}^b) \quad (4)$$

This equation has the desired shape of Eq. (1), i.e. the sum of the prior value and of a linear function of model-minus-measurement misfits. By construction, it does not depend on the retrieval prior  $\hat{\mathbf{x}}^b$ . However, to follow the optimal estimation framework, we still need to be able to develop the product of the gain matrices consistently with Eq. (2), i.e. like (neglecting errors in the observation operators):

$$\mathbf{K} = \hat{\mathbf{B}} \hat{\mathbf{H}}^T \check{\mathbf{H}}^T (\check{\mathbf{H}} \hat{\mathbf{H}} \hat{\mathbf{B}} \hat{\mathbf{H}}^T \check{\mathbf{H}}^T + \check{\mathbf{R}})^{-1} \quad (5)$$

In practice, we see that:

$$\hat{\mathbf{K}}' \check{\mathbf{K}} = \hat{\mathbf{B}} \hat{\mathbf{H}}'^T (\hat{\mathbf{H}}' \hat{\mathbf{B}} \hat{\mathbf{H}}'^T + \hat{\mathbf{R}}')^{-1} \check{\mathbf{B}} \check{\mathbf{H}}^T (\check{\mathbf{H}} \check{\mathbf{B}} \check{\mathbf{H}}^T + \check{\mathbf{R}})^{-1} \quad (6)$$

Eqs. (5-6) can be made consistent in general provided

$$\check{\mathbf{H}} \check{\mathbf{B}} \check{\mathbf{H}}^T = \check{\mathbf{H}} \hat{\mathbf{H}} \hat{\mathbf{B}} \hat{\mathbf{H}}^T \check{\mathbf{H}}^T \quad (7)$$

and (by developing  $\hat{\mathbf{H}}'$  and using Eq. (7))

$$\check{\mathbf{H}}^T \check{\mathbf{K}}^T (\check{\mathbf{K}} \check{\mathbf{H}} \check{\mathbf{B}} \check{\mathbf{H}}^T \check{\mathbf{K}}^T + \hat{\mathbf{R}}')^{-1} \check{\mathbf{B}} = \mathbf{I} \quad (8)$$

Equation (7) simply expresses consistency between the prior error statistics within the information content of the retrievals: the uncertainty of the retrieval prior and of the flux prior should be the same in radiance space. This condition is not achieved by current satellite retrieval algorithms, at least because they artificially maximize the measurement contribution in the retrievals through the use of very large prior error variances (see Section 2.1 or Butz et al. 2009, Reuter et al. 2010). However, if enough intermediate variables were saved by the retrieval schemes, it would be possible to reconstruct the retrievals with appropriate prior error variances and correlations.

Equation (8) can be satisfied in general if the retrieval averaging kernel  $\tilde{\mathbf{K}}\tilde{\mathbf{H}}$  is close to unity.. In practice, the retrieval averaging kernel for profiles is far from unity because current radiance measurements do not provide any vertical resolution for CO<sub>2</sub>. The situation is better if the state vector  $\mathbf{x}$  is the integrated column (in that case  $\tilde{\mathbf{H}}$  includes an operator to distribute the column in the vertical).

As a consequence of deviations from Eqs (7-8), the effective gain matrix  $\hat{\mathbf{K}}'\tilde{\mathbf{K}}$  significantly differs from the optimal one for GOSAT, resulting in a wrong balance between prior flux information and measured radiances. Overall,  $\tilde{\mathbf{K}}$  pulls too much towards the measured radiances and  $\hat{\mathbf{K}}'$  pulls too much towards the prior. This suboptimality very likely flaws the 4D information flow from the radiance measurements to the surface flux estimates. In particular, the suboptimality of  $\tilde{\mathbf{K}}$  affects the retrieval averaging kernel, that may not peak at the right height.

Migliorini (2012) proposed a sophisticated alternative to the averaging kernel assimilation of Connor et al. (1994), where the retrievals are assimilated after a linear transformation of both the retrievals and the observation operator. The transformation is heavier to implement than the above approach because it involves the retrieval signal-to-noise matrix  $\tilde{\mathbf{R}}^{-1/2}\tilde{\mathbf{H}}\tilde{\mathbf{B}}^{1/2}$ . It avoids the requirement of Eq. (8), but still requires consistent prior error statistics (Eq. (7)).

The situation complicates even further if we account for the facts that inversion systems assimilate bias-corrected retrievals (thereby implicitly re-introducing  $\mathbf{x}^b$  that had been neutralised by the use of averaging kernels, in the equations), that  $\tilde{\mathbf{H}}$  and  $\hat{\mathbf{H}}$  are imperfect operators, the uncertainty of which should be reported in  $\tilde{\mathbf{R}}$ , following Eq. (5), and that  $\tilde{\mathbf{H}}$  is usually non-linear. The need to report all observation operator uncertainties in  $\tilde{\mathbf{R}}$  means that retrieval configuration should in principle be tailored to the retrieval end-application, i.e. to the precision of the observation operator that is used in this end-application. For flux inversion, the transport model

uncertainty in  $XCO_2$  space is about 0.5 ppm (1  $\sigma$ , Houweling et al. 2010). When optimizing parameters of a flux model rather than for the flux themselves (in Carbon Cycle Data Assimilation Systems, Rayner et al. 2005), the uncertainty of the flux model equations has also to be reported in  $\tilde{R}$ : when projected in the space of  $XCO_2$ , they are comparable to transport model uncertainties (Kuppel et al. 2013).

## **4. Practical aspects**

Given the particular concerns raised about the optimality of  $XCO_2$  retrievals and of their averaging kernels in the previous section, we now focus on one specific retrieval product, ACOS-GOSAT, in order to look for some practical evidence of this sub-optimality.

### **4.1. Mean differences**

Fig. 1 shows the mean bias-corrected retrievals  $XCO_2^{a,c}$  and the mean corresponding posterior  $XCO_2$  field of the MACC inversion over the June 2009 – May 2013 period per  $3.75^\circ \times 1.9^\circ$  grid cell. All retrievals are used, provided they are found good by the ACOS standard quality control. The data density (Fig. 2b) follows the frequency of favourable retrieval conditions: more sunlight in the Tropics, less cloud over desert areas or over subsidence ocean regions. The long-term mean of the retrieval-minus-model differences (Fig. 2a) is usually about the ppm. Interestingly, it appears to be organized spatially. Over land, large positive values ( $> 0.5$  ppm, ACOS-GOSAT being larger) are seen over boreal forests, over most of South America, over grassland/cropland regions in Central Africa and over the West coast of the USA. Negative values occur over most of the other lands, with smaller values (up to  $\sim -1$  ppm) mostly over South and East Asia. Over

the oceans, values are mostly positive north of 30°N and south of 10°S, and negative in between. Both errors in ACOS-GOSAT and errors in the model simulations contribute to these differences, which complicates the interpretation of Fig. 2a. For instance, the zonal structure of the differences over the oceans could well be caused by the model, either because of too few surface air-sample sites in the Tropics or because the LMDZ transport model would not represent the inter-hemispheric exchange well enough (Patra et al. 2011). Alternatively, misrepresented clouds around the convergence zones could also induce them in the retrievals. Some of the patterns of Fig. 2a are similar to the surface cover, like the gradient between the Sahel and the African savannahs, or the one between the equatorial Atlantic and the African savannahs, while we expect the true XCO<sub>2</sub> fields to be first driven by large-scale horizontal advection (Keppel-Aleks et al. 2011). The main local spatial gradients in the mean differences are also seen on monthly means despite less data density (Fig. 3). They mostly reflect the retrieval gradients (Fig. 1a), because the model XCO<sub>2</sub> simulation is spatially smoother (Fig. 1b), even though it uses the retrieval averaging kernels (that change from scene to scene as a function, among other factors, of surface conditions) and even though it is sampled like the retrievals (i.e. with a spatially heterogeneous data density, also varying as a function, among other things, of surface conditions).

The jump of the long-term mean difference from the African savannahs to Sahel or equatorial Atlantic (while there is no jump between subtropical Atlantic and Western Sahara for instance) mostly corresponds to data from March (Fig. 3a), at the end of the savannah burning season (e.g. van der Werf et al. 2010). The model shows elevated values (Fig. 1b), but much less than the retrievals (Fig. 1a). If the model was underestimating the intensity of the fire, we would expect the mean difference to take the shape of a plume, i.e. to spread downstream the source region, but this is not the case. This suggests that the retrievals are affected by systematic errors over this region.

The positive differences of Fig. 2a in Eurasia notably follow the boreal forests, while negative values are found over the neighbouring regions of sparse tundra vegetation north of Siberia, or those of grassland/cropland south of them. The same remark applies to North America. The link with boreal forests is less obvious when looking at one isolated year because of the relatively small number of retrievals in these regions (not shown). The misfit pattern in Siberia and in North America contains many values larger than 1 ppm corresponding to relatively large retrieved XCO<sub>2</sub> (Fig. 1a). These large values are all the more surprising that retrievals in these high latitudes are obtained during the growing season and that boreal forests in Eurasia are identified as large carbon sinks by bottom-up inventories (Pan et al. 2011, Dolman et al. 2012). By comparison, we can look at agricultural regions, where the model could miss gradients during crop growth, both because the MACC inversion prior fluxes do not explicitly represent agricultural practices and because the location of the assimilated surface air-sample measurements only provides rough information about crop fluxes: the differences are marginal (-0.1 ppm on average, whether we compute the mean at the global scale or only for latitudes above 40°N) for retrievals located in crop regions, as identified by the high-resolution land cover map of ESA's Land Cover Climate Change Initiative project (<http://www.esa-landcover-cci.org/>). In the Corn Belt, the intensively agricultural region in the Midwest of the USA, differences are negative, but they are much smaller in absolute value (the differences are larger than -0.4 ppm) than over the boreal forests, and the Corn Belt boundaries do not sharply appear, in particular on its eastern side. The Corn Belt does not particularly appear in monthly means either (e.g., Fig. 3b). These elements suggest that the long-term mean differences over boreal forests come from a retrieval artifact rather than from the MACC inversion product.

From a radiative transfer point of view, boreal forests are largely covered with needle-leaved trees with low albedo in the strong CO<sub>2</sub> spectral band of GOSAT near 2.1  $\mu$ m (Fig. 4): these low

values hamper the  $\text{XCO}_2$  retrieval. O'Dell et al. (2012) already showed that large positive biases can occur for needle-leaved evergreen forests, with the retrieval exchanging surface albedo for very thin cloud or aerosol. Extreme cases are filtered out by the ACOS-GOSAT quality control, but Fig. 2a suggests that the remaining retrievals over boreal forests, including the region in Siberia East of  $100^\circ\text{E}$  which is dominated by deciduous needle-leaved trees with slightly larger albedos, are still biased. In temperate regions, south of  $50^\circ\text{N}$ , the differences for needle-leaf cover (mainly in Southeast USA and Southeast China) have the opposite sign, but they do not show up distinctly in the difference map like the boreal forests. Tropical forests in South America and in Africa also have low albedo and correspond to negative differences. They are more identifiable in Fig. 2a, but could be explained by an insufficient carbon sink in the model as well as by a retrieval artifact.

#### **4.2. Link to the retrieval increment**

We now look at the  $\text{XCO}_2$  misfit statistics over land and for the high-gain mode as a function of the size of the retrieval increment to its prior information ( $\text{XCO}_2^{\text{a}} - \text{XCO}_2^{\text{b}}$ ) in Fig. 5. We look at the misfits of the model to  $\text{XCO}_2^{\text{a}}$ , to  $\text{XCO}_2^{\text{a,c}}$  and to  $\text{XCO}_2^{\text{b}}$ , in order to visualize the added value brought by the retrieval process and by the bias correction, successively, on top of the prior estimate. This prior estimate about atmospheric  $\text{CO}_2$  has been provided to the retrieval scheme by a data-driven empirical model (Wunch et al. 2011a). In Fig. 5, each bin along the abscissa encompasses a large diversity of times during the four years and a large diversity of locations over the globe, over which the model simulation should be overall more accurate (smaller root mean square error) than  $\text{XCO}_2^{\text{b}}$ ,  $\text{XCO}_2^{\text{a}}$  and even  $\text{XCO}_2^{\text{a,c}}$  (Chevallier and O'Dell 2013). Further, we expect the model error to be uncorrelated with the error of  $\text{XCO}_2^{\text{b}}$ ,  $\text{XCO}_2^{\text{a}}$  and  $\text{XCO}_2^{\text{a,c}}$  so that

a smaller standard deviation of the misfits (e.g., using  $\text{XCO}_2^{\text{a}}$  rather than  $\text{XCO}_2^{\text{b}}$ ) can be interpreted in terms of better precision of the corresponding retrieval quantity.

The mean difference significantly varies with the increment size: starting at 0.7 ppm for the smallest increments it reaches about 2 ppm and -1 ppm, for  $\text{XCO}_2^{\text{b}}$  and  $\text{XCO}_2^{\text{a}}$  respectively. As expected, the mean difference is systematically better with  $\text{XCO}_2^{\text{a}}$  than with  $\text{XCO}_2^{\text{b}}$ . The bias correction ( $\text{XCO}_2^{\text{a,c}}$ ) further reduces the mean difference to a small extent.

The standard deviation for  $\text{XCO}_2^{\text{b}}$  is 1.1 ppm for small increments and smoothly increases to 2 ppm for retrieval increments of size 6 ppm. This trend demonstrates some skill of the retrieval algorithm to characterize the error of  $\text{XCO}_2^{\text{b}}$  from the GOSAT radiances and to generate a sizeable increment accordingly. By comparison, the model variability for a given increment size over the four years ranges between 3 and 4 ppm ( $1\sigma$ ), the prior variability is about 3 ppm and the retrieval variability ranges between 3 and 7 ppm. The standard deviation that uses  $\text{XCO}_2^{\text{a}}$  is 1.1 ppm for small increments. It smoothly increases to 4 ppm for retrieval increments of size 6 ppm: it is systematically larger than the standard deviation that uses  $\text{XCO}_2^{\text{b}}$  (despite a smaller mean difference). The standard deviation that uses  $\text{XCO}_2^{\text{a,c}}$  is also 1.1 ppm for small increments and is also systematically larger than the standard deviation that uses  $\text{XCO}_2^{\text{b}}$ , but it performs better than  $\text{XCO}_2^{\text{a}}$ . The worse standard deviation of the misfit of  $\text{XCO}_2^{\text{a}}$  and  $\text{XCO}_2^{\text{a,c}}$  to the model compared to  $\text{XCO}_2^{\text{b}}$  cannot be explained by a common lack of variability in the model and in  $\text{XCO}_2^{\text{b}}$  (that would correlate the model error with the that of  $\text{XCO}_2^{\text{b}}$ ), because (i) at the large scale, thinning the retrievals (for instance by keeping only one retrieval every nine model grid boxes for a given day) only marginally changes the figure (not shown), and (ii) at the sub-grid scale, the variability of  $\text{XCO}_2$  is usually well below the ppm (Alkhaled et al. 2008, Corbin et al. 2008), i.e. one order of magnitude smaller than the prior-to-retrieval degradation. Some, but not all, of the degradation is purely random and disappears after enough averaging (see Fig. 6 of Kulawik et al. 2015).



The fact that the standard deviation smoothly increases with increment size suggests that the increment size is systematically overestimated. Fig. 6 presents a simple test where we halve the retrieval increments, without any bias correction: we call  $\text{XCO}_2^{\text{a,r}} = \text{XCO}_2^{\text{b}} + (\text{XCO}_2^{\text{a}} - \text{XCO}_2^{\text{b}})/2$  the result. The reduction is seen to cancel most of the dependency of the statistics of the observation-minus-model misfits to the increment size: the standard deviation and the mean are then stable around 1.1 ppm and -0.3 ppm, respectively for increments up to 4 ppm without any bias correction. The standard deviation is systematically better than for  $\text{XCO}_2^{\text{b}}$ , which shows added value brought by the radiance measurements, in contrast to the previous results. This result also empirically confirms that the initial increments are in the right direction but are too large.

For the medium-gain retrievals (Fig. 7) and for the ocean glint retrievals (Fig. 8), the standard deviation of the misfits using  $\text{XCO}_2^{\text{a,c}}$  is not significantly larger than that using  $\text{XCO}_2^{\text{b}}$ .

## 5. Discussion and conclusions

Small uncertainties in aerosols, cirrus cloud or surface albedo are known to heavily affect the quality of the  $\text{XCO}_2$  satellite retrievals and to propagate into biases in the fluxes inverted from them, even when the parasite signal in  $\text{XCO}_2$  is sub-ppm. This weakness lead the science team of NASA's OCO, a satellite that failed at launch in February 2009, to conclude that the space-based NIR/SWIR measurements of  $\text{XCO}_2$  could not be used alone for  $\text{CO}_2$  source-sink inversions and that they had to be combined with observations from a reasonable number of surface stations (Miller et al. 2007). However, so much improvement has been obtained in these issues by various institutes during the last few years, that it is sometimes thought that the space-borne  $\text{XCO}_2$  retrievals have reached sufficient quality for source-sink inversion. The present paper discusses

where we stand in this respect both from general theoretical considerations and from one of the most advanced GOSAT retrieval products.

From the theory, we have shown that a two-step approach to infer the surface fluxes from the GOSAT measured radiances, with CO<sub>2</sub> retrievals as an intermediate product, cannot be optimal. This suboptimality corrupts the 4D information flow from the radiance measurements to the surface flux estimates. It is amplified by the current retrieval strategy where prior errors are much larger (by an order of magnitude in terms of variances) than the performance of prior CO<sub>2</sub> simulations used in atmospheric inversions. Indeed, the use of averaging kernels makes atmospheric inversion insensitive to the choice of a particular retrieval prior CO<sub>2</sub> profile (Connor et al. 1994) if retrievals are assimilated without any bias correction, but it does not make the retrieval prior error statistics disappear from the inverse modelling equations. The current strategy likely generates retrieval averaging kernels that are inappropriate for atmospheric inversions in their default configurations, with a wrong vertical distribution and an excessive weight towards the measured radiances. Paradoxically, empirical bias correction of the retrievals (e.g., Wunch et al., 2011b) also contributes to the degradation of the 4D information flow, because it carries the imprint of the retrieval prior and of the retrieval prior error statistics. Direct assimilation of the measured radiances would solve the inconsistency, but would increase the computational burden of atmospheric inversions by several orders of magnitude. Alternatively, we could adapt the inversion systems to the current retrieval configuration by using minimal prior information about the surface fluxes, typically a flat prior flux field, but the result would still over-fit the measured radiances due to the absence of other (compensating) information.

We have compared the ACOS-GOSAT retrievals with a transport model simulation constrained by surface air-sample measurements in order to find some evidence of retrieval sub-optimality. Flaws in this transport model and in these inverted surface fluxes necessarily flaw the

simulation in many places over the globe and at various times of the year. We therefore carefully selected some of the relatively large discontinuities in the  $\text{XCO}_2$  fields that the simulation unlikely generated. We found some evidence of retrieval systematic errors over the dark surfaces of the high-latitude lands and over African savannahs. We note that the mean differences over the African savannahs during the burning season could be explained by retrieval averaging kernels not peaking low enough in the atmosphere further to the assignment of inappropriate prior error correlations. Biomass burning aerosols that would not be well identified by the retrieval scheme could also play a role. We also found some evidence that the high-gain retrievals over land systematically over-fit the measured radiances, as a consequence of the prior uncertainty overestimation and of an underestimation of the observation uncertainty (as seen by the underlying radiative transfer model). This over-fit is partially compensated by the bias correction. An empirical test indicates that halving the retrieval increments without any posterior bias correction actually cancels the dependency of the statistics of the observation-minus-model misfits to the increment size and makes the standard deviation systematically better than for the retrieval prior  $\text{XCO}_2^b$ , which shows added value brought by the radiance measurements, in contrast to the previous results. We argue here that the optimal-estimation retrieval process and, consequently, its posterior bias correction need retuning.

Given the diversity of existing satellite retrieval algorithms, our conclusions cannot be easily extrapolated to other GOSAT retrieval products and even less to  $\text{XCO}_2$  retrievals from other instruments, but we note that such mistuning like the one highlighted here is common practice, both because the errors of the retrieval forward model are difficult to characterize and because satellite retrievals are usually explicitly designed to maximize the observation contribution, at the risk of over-fitting radiance and forward model noise. A primary consequence of this mistuning is the usual underestimation of retrieval errors: for instance, O'Dell et al. (2012) recommended

inflating this error by a twofold factor for ACOS-GOSAT b2.8. More importantly, our results show that the mistuning generates excessive (unphysical) space-time variations of the retrievals up to ~1%. This noise level would not matter for short-lived species, but for CO<sub>2</sub> it is enough to significantly degrade the assimilation of the retrievals for flux inversion and may explain some of the inconsistency seen between GOSAT-based top-down results and bottom-up results for CO<sub>2</sub> (Chevallier et al. 2014, Reuter et al. 2014). Therefore, with the current mistuning, we reiterate previous recommendations to take GOSAT-based CO<sub>2</sub> inversion results particularly cautiously. But we also suggest that this situation may dramatically improve by simply retuning the retrieval schemes. Ultimately, internal statistical consistency of the retrievals and of the inversion schemes is needed to establish the credibility of their end product.

## Acknowledgements

Some of this work was performed using HPC resources of DSM-CCRT and of CCRT under the allocation t2014012201 made by GENCI (Grand Équipement National de Calcul Intensif). It was co-funded by the European Commission under the EU H2020 Programme (grant agreement No. 630080, MACC III). The ACOS GOSAT data can be obtained from <http://co2.jpl.nasa.gov>. They were produced by the ACOS/OCO-2 project at the Jet Propulsion Laboratory, California Institute of Technology, using GOSAT observed spectral radiances made available by the GOSAT project. The MACC product can be obtained from <http://www.copernicus-atmosphere.eu>. The author is very grateful to the many people involved in the surface CO<sub>2</sub> measurements and in the archiving of these data that were kindly made available to him. He thanks C. O'Dell for many fruitful and stimulating discussions about the topics addressed here. He also benefitted from interesting feedback from two anonymous reviewers and from Grégoire Broquet, Junjie Liu, Noel

457 Cressie, Sourish Basu, Kevin W. Bowman and Susan Kulawik in the discussion phase of the  
458 paper.

459

460 **References**

461 Aben, I., Hasekamp, O., and Hartmann, W.: Uncertainties in the space-based measurements of  
462 CO<sub>2</sub> columns due to scattering in the Earth's atmosphere, *J. Quant. Spectrosc. Radiat. Trans.*,  
463 104(3), 450–459, 2007

464 Alkhaled, A. A., Michalak, A. M., and Kawa, S. R.: Using CO<sub>2</sub> spatial variability to quantify  
465 representation errors of satellite CO<sub>2</sub> retrievals, *Geophys. Res. Lett.*, 35, L16813,  
466 doi:10.1029/2008GL034528, 2008.

467 Basu, S., Guerlet, S., Butz, A., Houweling, S., Hasekamp, O., Aben, I., Krummel, P., Steele, P.,  
468 Langenfelds, R., Torn, M., Biraud, S., Stephens, B., Andrews, A., and Worthy, D.: Global CO<sub>2</sub>  
469 fluxes estimated from GOSAT retrievals of total column CO<sub>2</sub>, *Atmos. Chem. Phys.*, 13, 8695-  
470 8717, doi:10.5194/acp-13-8695-2013, 2013.

471 Basu, S., M. Krol, A. Butz, C. Clerbaux, Y. Sawa, T. Machida, H. Matsueda, C. Frankenberg, O.  
472 P. Hasekamp, and I. Aben, The seasonal variation of the CO<sub>2</sub> flux over Tropical Asia estimated  
473 from GOSAT, CONTRAIL, and IASI, *Geophys. Res. Lett.*, 41, 1809–1815,  
474 doi:10.1002/2013GL059105, 2014.

475 Boesch, H., Toon, G. C., Sen, B., Washenfelder, R. A., Wennberg, P. O., Buchwitz, M., de Beek,  
476 R., Burrows, J. P., Crisp, D., Christi, M., Connor, B. J., Natraj, V., and Yung, Y. L.: Space-  
477 based near-infrared CO<sub>2</sub> measurements: Testing the Orbiting Carbon Observatory retrieval  
478 algorithm and validation concept using SCIAMACHY observations over Park Falls, Wisconsin,  
479 *J. Geophys. Res. Atmos.*, 111, D23302, doi:10.1029/2006JD007080, 2006.

480 Buchwitz, M., de Beek, R., Burrows, J. P., Bovensmann, H., Warneke, T., Notholt, J.,  
 481 Meirink, J. F., Goede, A. P. H., Bergamaschi, P., Körner, S., Heimann, M., and Schulz, A.:  
 482 Atmospheric methane and carbon dioxide from SCIAMACHY satellite data: initial comparison  
 483 with chemistry and transport models, *Atmos. Chem. Phys.*, 5, 941-962, doi:10.5194/acp-5-941-  
 484 2005, 2005.

485 Butz, A., Hasekamp, O. P., Frankenberg, C., and Aben, I.: Retrievals of atmospheric CO<sub>2</sub> from  
 486 simulated space-borne measurements of backscattered near-infrared sunlight: accounting for  
 487 aerosol effects, *Appl. Opt.*, 48, 3322–3336, doi:10.1364/AO.48.003322, 2009

488 Chédin, A., Serrar, S., Scott, N. A., Crevoisier, C., and Armante, R.: First global measurement of  
 489 midtropospheric CO<sub>2</sub> from NOAA polar satellites: Tropical zone, *J. Geophys. Res.*, 108(D18),  
 490 4581, doi:10.1029/2003JD003439, 2003..

491 Chevallier, F., Fisher, M., Peylin, P., Serrar, S., Bousquet, P., Bréon, F.-M., Chédin, A., and Ciais,  
 492 P.: Inferring CO<sub>2</sub> sources and sinks from satellite observations: method and application to  
 493 TOVS data, *J. Geophys. Res.*, 110, D24309, doi:10.1029/2005JD006390, 2005.

494 Chevallier, F.: Impact of correlated observation errors on inverted CO<sub>2</sub> surface fluxes from OCO  
 495 measurements, *Geophys. Res. Lett.*, 34, L24804, doi:10.1029/2007GL030463, 2007.

496 Chevallier, F., Bréon, F.-M., and Rayner, P. J.: The contribution of the Orbiting Carbon  
 497 Observatory to the estimation of CO<sub>2</sub> sources and sinks: Theoretical study in a variational data  
 498 assimilation framework. *J. Geophys. Res.*, 112, D09307, doi:10.1029/2006JD007375, 2007.

499 Chevallier, F., Ciais, P., Conway, T. J., Aalto, T., Anderson, B. E., Bousquet, P., Brunke, E. G.,  
 500 Ciattaglia, L., Esaki, Y., Fröhlich, M., Gomez, A., Gomez-Pelaez, A. J., Haszpra, L., Krummel,  
 501 P. B., Langenfelds, R. L., Leuenberger, M., Machida, T., Maignan, F., Matsueda, H., Morgui, J.

502 A., Mukai, H., Nakazawa, T., Peylin, P., Ramonet, M., Rivier, L., Sawa, Y., Schmidt, M.,  
 503 Steele, L. P., Vay, S. A., Vermeulen, A. T., Wofsy, S., and Worthy, D.: CO<sub>2</sub> surface fluxes at  
 504 grid point scale estimated from a global 21-year reanalysis of atmospheric measurements. *J.*  
 505 *Geophys. Res.*, 115, D21307, doi:10.1029/2010JD013887, 2010.  
 506

507 Chevallier, F., and O'Dell, C. W., Error statistics of Bayesian CO<sub>2</sub> flux inversion schemes as seen  
 508 from GOSAT. *Geophys. Res. Lett.*, 40, 1252–1256, doi:10.1002/grl.50228, 2013.

509 Chevallier, F., Palmer, P. I., Feng, L., Boesch, H., O'Dell, C. W., and Bousquet, P.: Towards  
 510 robust and consistent regional CO<sub>2</sub> flux estimates from in situ and space-borne measurements  
 511 of atmospheric CO<sub>2</sub>, *Geophys. Res. Lett.*, 41, 1065–1070, doi:10.1002/2013GL058772, 2014.

512 Connor, B. J., Siskind, D. E., Tsou, J. J., Parrish, A., and Remsberg, E. E.: Ground-based  
 513 microwave observations of ozone in the upper stratosphere and mesosphere, *J. Geophys. Res.*,  
 514 99, 16,757–16,770, 1994.

515 Connor, B. J., Boesch, H., Toon, G., Sen, B., Miller, C., and Crisp, D.: Orbiting Carbon  
 516 Observatory: Inverse method and prospective error analysis, *J. Geophys. Res. Atmos.*, 113,  
 517 D05305, doi:10.1029/2006JD008336, 2008.

518 Corbin, K., Denning, A. S., Wang, J.-W., Lu, L., and Baker, I. T.: Possible representation errors  
 519 in inversions of satellite CO<sub>2</sub> retrievals, *J. Geophys. Res.*, 113, D02301,  
 520 doi:10.1029/2007JD008716, 2008.

521 Crisp, D., Fisher, B. M., O'Dell, C., Frankenberg, C., Basilio, R., Bösch, H., Brown, L. R.,  
 522 Castano, R., Connor, B., Deutscher, N. M., Eldering, A., Griffith, D., Gunson, M., Kuze, A.,  
 523 Mandrake, L., McDuffie, J., Messerschmidt, J., Miller, C. E., Morino, I., Natraj, V., Notholt, J.,



524 O'Brien, D. M., Oyafuso, F., Polonsky, I., Robinson, J., Salawitch, R., Sherlock, V., Smyth, M.,  
525 Suto, H., Taylor, T. E., Thompson, D. R., Wennberg, P. O., Wunch, D., and Yung, Y. L.: The  
526 ACOS CO<sub>2</sub> retrieval algorithm – Part II: Global XCO<sub>2</sub> data characterization,  
527 Atmos. Meas. Tech., 5, 687–707, doi:10.5194/amt-5-687-2012, 2012.

528 Dolman, A. J., Shvidenko, A., Schepaschenko, D., Ciais, P., Tchepakova, N., Chen, T.,  
529 van der Molen, M. K., Belelli Marchesini, L., Maximov, T. C., Maksyutov, S., and Schulze, E.-  
530 D.: An estimate of the terrestrial carbon budget of Russia using inventory-based, eddy  
531 covariance and inversion methods, Biogeosciences, 9, 5323-5340, doi:10.5194/bg-9-5323-2012,  
532 2012.

533 Engelen, R. J., Serrar, S., and Chevallier, F.: Four-dimensional data assimilation of atmospheric  
534 CO<sub>2</sub> using AIRS observations, J. Geophys. Res., 114, D03303, doi:10.1029/2008JD010739,  
535 2009.

536 Global Climate Observing System (GCOS), Systematic observation requirements for satellite-  
537 based products for climate, Supplemental details to the satellite-based component of the  
538 “Implementation Plan for the Global Observing System for Climate in Support of the UNFCCC  
539 (2010 update)”, Prepared by World Meteorological Organization (WMO), Intergovernmental  
540 Oceanographic Commission, United Nations Environment Programme (UNEP), International  
541 Council for Science, Doc.: GCOS 154, 2010.

542 Guerlet, S., S. Basu, A. Butz, M. C. Krol, P. Hahne, S. Houweling, O. P. Hasekamp, and I. Aben,  
543 Reduced carbon uptake during the 2010 Northern Hemisphere summer as observed from  
544 GOSAT, Geophys. Res. Lett., 40, 2378–2383, doi:10.1002/grl.50402, 2013a.

545 Guerlet, S., Butz, A., Schepers, D., Basu, S., Hasekamp, O. P., Kuze, A., Yokota, T., Blavier, J.-  
546 F., Deutscher, N. M., Griffith, D. W. T., Hase, F., Kyrö, E., Morino, I., Sherlock, V., Sussmann,

547 R., Galli, A., and Aben, I.: Impact of aerosol and thin cirrus on retrieving and validating XCO<sub>2</sub>  
548 from GOSAT shortwave infrared measurements, *J. Geophys. Res. Atmos.*, 118, 4887–4905,  
549 doi:10.1002/jgrd.50332, 2013b.

550 Hourdin, F., Musat, I., Bony, S., Braconnot, P., Codron, F., Dufresne, J. L., Fairhead, L., Filiberti,  
551 M. A., Friedlingstein, P., Grandpeix, J. Y., Krinner, G., Levan, P., Li, Z. X., and Lott, F.: The  
552 LMDZ4 general circulation model: climate performance and sensitivity to parametrized physics  
553 with emphasis on tropical convection, *Climate Dynamics*, 27, 787–813, doi:10.1007/s00382-  
554 006-0158-0, 2006.

555 Houweling, S., Aben, I., Breon, F.-M., Chevallier, F., Deutscher, N., Engelen, R., Gerbig, C.,  
556 Griffith, D., Hungershoefer, K., Macatangay, R., Marshall, J., Notholt, J., Peters, W., and  
557 Serrar, S.: The importance of transport model uncertainties for the estimation of CO<sub>2</sub> sources  
558 and sinks using satellite measurements, *Atmos. Chem. Phys.*, 10, 9981–9992, doi:10.5194/acp-  
559 10-9981-2010, 2010.

560 Ingmann, P.: A-SCOPE, Advanced Space Carbon and Climate Observation of Planet Earth,  
561 Report of Assessment, SP-1313/1, ESA Communication Product Office, Noordwijk, The  
562 Netherlands, 2009.

563 Keppel-Aleks, G., Wennberg, P. O., and Schneider, T.: Sources of variations in total column  
564 carbon dioxide, *Atmos. Chem. Phys.*, 11, 3581–3593, doi:10.5194/acp-11-3581-2011, 2011.

565 Kulawik, S. S., Wunch, D., O'Dell, C., Frankenberg, C., Reuter, M., Oda, T., Chevallier, F.,  
566 Sherlock, V., Buchwitz, M., Osterman, G., Miller, C., Wennberg, P., Griffith, D. W. T.,  
567 Morino, I., Dubey, M., Deutscher, N. M., Notholt, J., Hase, F., Warneke, T., Sussmann, R.,  
568 Robinson, J., Strong, K., Schneider, M., and Wolf, J.: Consistent evaluation of GOSAT,

569 SCIAMACHY, CarbonTracker, and MACC through comparisons to TCCON, *Atmos. Meas.*  
 570 *Tech. Discuss.*, 8, 6217-6277, doi:10.5194/amtd-8-6217-2015, 2015.

571 Kuppel, S., Chevallier, F. and Peylin, P.: Quantifying the model structural error in Carbon Cycle  
 572 Data Assimilation Systems. *Geosci. Model Dev.*, 6, 45-55, doi:10.5194/gmd-6-45-2013, 2013.

573 Maksyutov, S., Kadygrov, N., Nakatsuka, Y., Patra, P. K., Nakazawa, T., Yokota, T. and Inoue,  
 574 G.: Projected impact of the GOSAT observations on regional CO<sub>2</sub> flux estimations as a function  
 575 of total retrieval error, *J. Remote Sens. Soc. Jpn.*, 28, 190–197, 2008.

576 Migliorini, S.: On the equivalence between radiance and retrieval assimilation. *Mon. Wea. Rev.*,  
 577 140, 258-265. doi:10.1175/MWR-D-10-05047.1, 2012.

578 Miller, C. E., Crisp, D., DeCola, P. L., Olsen, S. C., Randerson, J. T., Michalak, A. M., Alkhaled,  
 579 A., Rayner, P., Jacob, D. J., Suntharalingam, P., Jones, D. B. A., Denning, A. S., Nicholls, M.  
 580 E., Doney, S. C., Pawson, S., Boesch, H., Connor, B. J., Fung, I. Y., O'Brien, D., Salawitch, R.  
 581 J., Sander, S. P., Sen, B., Tans, P., Toon, G. C., Wennberg, P. O., Wofsy, S. C., Yung, Y. L.,  
 582 and Law, R. M.: Precision requirements for space-based XCO<sub>2</sub> data, *J. Geophys. Res.*, 112,  
 583 D10314, doi:10.1029/2006JD007659, 2007.

584 Nguyen, H., Osterman, G., Wunch, D., O'Dell, C., Mandrake, L., Wennberg, P., Fisher, B., and  
 585 Castano, R.: A method for colocating satellite XCO<sub>2</sub> data to ground-based data and its  
 586 application to ACOS-GOSAT and TCCON, *Atmos. Meas. Tech.*, 7, 2631-2644,  
 587 doi:10.5194/amt-7-2631-2014, 2014.

588 O'Dell, C. W., Connor, B., Bösch, H., O'Brien, D., Frankenberg, C., Castano, R., Christi, M.,  
 589 Eldering, D., Fisher, B., Gunson, M., McDuffie, J., Miller, C. E., Natraj, V., Oyafuso, F.,  
 590 Polonsky, I., Smyth, M., Taylor, T., Toon, G. C., Wennberg, P. O., and Wunch, D.: The ACOS  
 591 CO<sub>2</sub> retrieval algorithm – Part 1: Description and validation against synthetic observations,  
 592 *Atmos. Meas. Tech.*, 5, 99–121, doi:10.5194/amt-5-99-2012, 2012.

593 Oshchepkov, S., Bril, A., Yokota, T., Wennberg, P. O., Deutscher, N. M., Wunch, D., Toon, G.  
 594 C., Yoshida, Y., O'Dell, C. W., Crisp, D., Miller, C. E., Frankenberg, C., Butz, A., Aben, I.,  
 595 Guerlet, S., Hasekamp, O., Boesch, H., Cogan, A., Parker, R., Griffith, D., Macatangay, R.,  
 596 Notholt, J., Sussmann, R., Rettinger, M., Sherlock, V., Robinson, J., Kyrö, E., Heikkinen, P.,  
 597 Feist, D. G., Morino, I., Kadyrov, N., Belikov, D., Maksyutov, S., Matsunaga, T., Uchino, O.,  
 598 and Watanabe, H.: Effects of atmospheric light scattering on spectroscopic observations of  
 599 greenhouse gases from space. Part 2: Algorithm intercomparison in the GOSAT data processing  
 600 for CO<sub>2</sub> retrievals over TCCON sites, J. Geophys. Res., 118, 1493-1512,  
 601 doi:10.1002/jgrd.50146, 2013.

602 Osterman, G., Eldering, A., Avis, C., O'Dell, C., Martinez, E., Crisp, D., Frankenberg, C., and  
 603 Frankenberg, B., ACOS Level 2 Standard Product Data User's Guide v3.4, Revision Date:  
 604 Revision B, 3 October 2013, available at:  
 605 [https://co2.jpl.nasa.gov/static/docs/v3.4\\_DataUsersGuide-RevB\\_131028.pdf](https://co2.jpl.nasa.gov/static/docs/v3.4_DataUsersGuide-RevB_131028.pdf) (last access: 20  
 606 April 2015), 2013.

607 Pan, Y., Birdsey, R. A., Fang, J., Houghton, R., Kauppi, P. E., Kurz, W. A., Phillips, O. L.,  
 608 Shvidenko, A., Lewis, S. L., Canadell, J. G., Ciais, P., Jackson, J. B., Pacala, S., McGuire, A.  
 609 D., Piao, S., Rautiainen, A., Sitch, S., and Hayes, D.: A large and persistent carbon sink in the  
 610 world's forests, Science, 333, 988–993, 2011.

611 Patra, P. K., Houweling, S., Krol, M., Bousquet, P., Belikov, D., Bergmann, D., Bian, H.,  
 612 Cameron-Smith, P., Chipperfield, M. P., Corbin, K., Fortems-Cheiney, A., Fraser, A., Gloor, E.,  
 613 Hess, P., Ito, A., Kawa, S. R., Law, R. M., Loh, Z., Maksyutov, S., Meng, L., Palmer, P. I.,  
 614 Prinn, R. G., Rigby, M., Saito, R., and Wilson, C.: TransCom model simulations of CH<sub>4</sub> and  
 615 related species: linking transport, surface flux and chemical loss with CH<sub>4</sub> variability in the

616 troposphere and lower stratosphere, *Atmos. Chem. Phys.*, 11, 12813-12837, doi:10.5194/acp-  
617 11-12813-2011, 2011..

618 Peng, S., Ciais, P., Chevallier, F., Peylin, P., Cadule, P., Sitch, S., Piao, S., Ahlström, A.,  
619 Huntingford, C., Levy, P., Li, X., Liu, Y., Lomas, M., Poulter, B., Viovy, N., Wang, T., Wang,  
620 X., Zaehle, S., Zeng, N., Zhao, F., and Zhao, H.: Benchmarking the seasonal cycle of CO<sub>2</sub>  
621 fluxes simulated by terrestrial ecosystem models, *Global Biogeochem. Cycles*, 29, 46–64,  
622 doi:10.1002/2014GB004931, 2015.

623 Peylin, P., Law, R. M., Gurney, K. R., Chevallier, F., Jacobson, A. R., Maki, T., Niwa, Y.,  
624 Patra, P. K., Peters, W., Rayner, P. J., Rödenbeck, C., van der Laan-Luijkx, I. T., and  
625 Zhang, X.: Global atmospheric carbon budget: results from an ensemble of atmospheric CO<sub>2</sub>  
626 inversions, *Biogeosciences*, 10, 6699-6720, doi:10.5194/bg-10-6699-2013, 2013.

627 Rayner, P., Scholze, M., Knorr, W., Kaminski, T., Giering, R., and Widmann, H.: Two decades  
628 of terrestrial Carbon fluxes from a Carbon Cycle Data Assimilation System (CCDAS), *Global*  
629 *Biogeochem. Cy.*, 19, GB2026, doi:10.1029/2004GB002254, 2005

630 Reuter, M., Buchwitz, M., Schneising, O., Heymann, J., Bovensmann, H., and Burrows, J. P.: A  
631 method for improved SCIAMACHY CO<sub>2</sub> retrieval in the presence of optically thin clouds,  
632 *Atmos. Meas. Tech.*, 3, 209-232, doi:10.5194/amt-3-209-2010, 2010.

633 Reuter, M., Buchwitz, M., Hilker, M., Heymann, J., Schneising, O., Pillai, D., Bovensmann, H.,  
634 Burrows, J. P., Bösch, H., Parker, R., Butz, A., Hasekamp, O., O'Dell, C. W., Yoshida, Y.,  
635 Gerbig, C., Nehrkorn, T., Deutscher, N. M., Warneke, T., Notholt, J., Hase, F., Kivi, R.,  
636 Sussmann, R., Machida, T., Matsueda, H., and Sawa, Y.: Satellite-inferred European carbon  
637 sink larger than expected, *Atmos. Chem. Phys.*, 14, 13739–13753, doi:10.5194/acp-14-13739-  
638 2014, 2014.

Rodgers, C.D.: Inverse Methods for Atmospheric Sounding: Theory and Practice, World Scientific Publishing Co. Ltd., London, 2000.

van der Werf, G. R., Randerson, J. T., Giglio, L., Collatz, G. J., Mu, M., Kasibhatla, P. S., Morton, D. C., DeFries, R. S., Jin, Y., and van Leeuwen, T. T.: Global fire emissions and the contribution of deforestation, savanna, forest, agricultural, and peat fires (1997–2009), *Atmos. Chem. Phys.*, 10, 11,707–11,735, doi:10.5194/acp-10-11707-2010, 2010.

Wunch, D., Toon, G. C., Blavier, J.-F. L., Washenfelder, R. A., Notholt, J., Connor, B. J., Griffith, D. W. T., Sherlock, V., and Wennberg, P. O., The Total Carbon Column Observing Network, *Phil. Trans. R. Soc. A*:2011369 2087–2112;DOI: 10.1098/rsta.2010.0240, 2011a.

Wunch, D., Wennberg, P. O., Toon, G. C., Connor, B. J., Fisher, B., Osterman, G. B., Frankenberg, C., Mandrake, L., O'Dell, C., Ahonen, P., Biraud, S. C., Castano, R., Cressie, N., Crisp, D., Deutscher, N. M., Eldering, A., Fisher, M. L., Griffith, D. W. T., Gunson, M., Heikkinen, P., Keppel-Aleks, G., Kyrö, E., Lindenmaier, R., Macatangay, R., Mendonca, J., Messerschmidt, J., Miller, C. E., Morino, I., Notholt, J., Oyafuso, F. A., Rettinger, M., Robinson, J., Roehl, C. M., Salawitch, R. J., Sherlock, V., Strong, K., Sussmann, R., Tanaka, T., Thompson, D. R., Uchino, O., Warneke, T., and Wofsy, S. C.: A method for evaluating bias in global measurements of CO<sub>2</sub> total columns from space, *Atmos. Chem. Phys.*, 11, 12317–12337, doi:10.5194/acp-11-12317-2011, 2011b.

<b>Locality (identifier)</b>	<b>Period</b>	<b>Source</b>
Alert, Nunavut, CA (ALT)	1988-2012	WDCGG/ EC
Amsterdam Island, FR (AMS)	1981-2011	LSCE
Argyle, Maine, US (AMT)	2003-2011	NOAA/ ESRL
Anmyeon-do, KR (AMY)	1999-2012	WDCGG/ KMA
Barrow, Alaska, US (BRW)	1979-2013	NOAA/ ESRL
Candle Lake, CA (CDL)	2002-2012	WDCGG/ EC
Monte Cimone, IT (CMN)	1996-2010	WDCGG/ IAFMS
Cape Ochi-ishi, JP (COI)	1995-2002	WDCGG/ NIES
Cape Point, SA (CPT)	1993-2013	WDCGG/ SAWS
Egbert, CA (EGB)	2005-2012	WDCGG/ EC
East Trout Lake, CA (ETL)	2005-2012	WDCGG/ EC
Frasedale, CA (FSD)	1990-2012	WDCGG/ EC
Hateruma, JP (HAT)	1993-2002	WDCGG/ NIES
Hegyhatsal tower, 115m level, HU (HUN0115)	1994-2013	WDCGG/ HMS
Tenerife, Canary Islands, ES (IZO)	1984-2013	WDCGG/ AEMET
Jubany, Antartica, AR (JBN)	1994-2009	WDCGG/ ISAC IAA WDCGG/ Univ. Of
Jungfraujoch, CH (JFJ)	2004-2013	Bern
K-puszt, HU (KPS)	1981-1999	WDCGG/ HMS
Park Falls, Wisconsin, US (LEF)	2003-2011	NOAA/ ESRL
Mace Head, County Galway, IE (MHD)	1992-2012	LSCE

Mauna Loa, Hawaii, US (MLO)	1979-2013	NOAA/ ESRL
Minamitorishima, JP (MNM)	1993-2013	WDCGG/ JMA
Pallas-Sammaltunturi, GAW Station, FI (PAL)	1999-2013	WDCGG/ FMI WDCGG/ CESI
Plateau Rosa, IT (PRS)	2000-2013	RICERCA
Puy de Dome, FR (PUY)	2000-2010	LSCE
Ryori, JP (RYO)	1987-2013	WDCGG/ JMA
Tutuila, American Samoa (SMO)	1979-2013	NOAA/ ESRL
Sonnblick, AU (SNB)	1999-2013	WDCGG/ EEA
South Pole, Antarctica, US (SPO)	1979-2013	NOAA/ ESRL
Tsukuba tower, 200m level, JP (TKB)	1986-2000	WDCGG/ MRI
Westerland, DE (WES)	1979-2013	WDCGG/ UBA
Moody, Texas, US (WKT)	2003-2011	NOAAA/ ESRL
Yonagunijima, JP (YON)	1997-2013	WDCGG/ JMA

659

660 **Table 1: List of the continuous sites used in the MACC CO<sub>2</sub> inversion v13r1 together with**

661 **the period of coverage (defined as the period between the first sample and the last one), and**

662 **the data source. Each station is identified by the name of the place, the corresponding**

663 **country (abbreviated) and the code used in the corresponding database.**

664



<b>Locality (identifier)</b>	<b>Period</b>	<b>Source</b>
Alert, Nunavut, CA (ALT)	1985-2013	NOAA/ ESRL
Amsterdam Island, FR (AMS)	1979-1990	NOAA/ ESRL
Amsterdam Island, FR (AMS)	2003-2013	LSCE
Ascension Island, GB (ASC)	1979-2013	NOAA/ ESRL
Assekrem, DZ (ASK)	1995-2013	NOAA/ ESRL
St. Croix, Virgin Islands, USA		
(AVI)	1979-1990	NOAA/ ESRL
Terceira Island, Azores, PT (AZR)	1979-2013	NOAA/ ESRL
Baltic Sea, PL (BAL)	1992-2011	NOAA/ ESRL
Bering Island, RU (BER)	1986-1994	WDCGG/ MGO
Begur, ES (BGU)	2000-2013	LSCE /IC3
Baring Head, NZ (BHD)	1999-2013	NOAA/ESRL
Baring Head, NZ (BHD)	1979-2011	WDCGG/ NIWA
Bukit Kototabang, ID (BKT)	2004-2013	NOAA/ESRL
St. Davids Head, Bermuda, GB		
(BME)	1989-2009	NOAA/ ESRL
Tudor Hill, Bermuda, GB (BMW)	1989-2013	NOAA/ ESRL
Barrow, Alaska, US (BRW)	1979-2013	NOAA/ ESRL
Portsall, FR (BZH)	1998-2001	CarboEurope/LSCE
Cold Bay, Alaska, US (CBA)	1979-2013	NOAA/ ESRL
Cape Ferguson, AU (CFA)	1991-2013	WDCGG/ CSIRO
Cape Grim, Tasmania, AU (CGO)	1984-2013	NOAA/ ESRL
Christmas Island, Republic of		
Kiribati (CHR)	1984-2013	NOAA/ ESRL

Cape Meares, Oregon, US (CMO)	1982-1998	NOAA/ ESRL
Crozet Island, FR (CRZ)	1991-2013	NOAA/ ESRL
Cape St. James, CA (CSJ)	1979-1992	WDCGG/ EC
Casey Station, AU (CYA)	1996-2013	WDCGG/ CSIRO
Drake Passage (DRP)	2003-2013	NOAA/ ESRL
Easter Island, CL (EIC)	1994-2013	NOAA/ ESRL
Estevan Point, British Columbia, CA (ESP)	1992-2012	WDCGG/ EC
Estevan Point, British Columbia, CA (ESP)	1993-2001	WDCGG/ CSIRO
Finokalia, Crete, GR (FIK)	1999-2013	LSCE
Mariana Islands, Guam (GMI)	1979-2013	NOAA/ ESRL
Dwejra Point, Gozo, MT (GOZ)	1993-1999	NOAA/ ESRL
Halley Station, Antarctica, GB (HBA)	1983-2013	NOAA/ ESRL
Hohenpeissenberg, DE (HPB)	2006-2013	NOAA/ ESRL
Hegyhatsal, HU (HUN)	1993-2013	NOAA/ ESRL
Storhofdi, Vestmannaeyjar, IS (ICE)	1992-2013	NOAA/ ESRL
Grifton, North Carolina, US (ITN)	1992-1999	WDCGG/ ESRL
Tenerife, Canary Islands, ES (IZO)	1991-2013	NOAA/ ESRL
Key Biscayne, Florida, US (KEY)	1979-2013	NOAA/ ESRL
Kotelny Island, RU (KOT)	1986-1993	WDCGG/ MGO
Cape Kumukahi, Hawaii, US (KUM)	1979-2013	NOAA/ ESRL

Sary Taukum, KZ (KZD)	1997-2009	NOAA/ ESRL
Plateau Assy, KZ (KZM)	1997-2009	NOAA/ ESRL
Lulin, TW (LLN)	2006-2013	NOAA/ ESRL
Lampedusa, IT (LMP)	2006-2013	NOAA/ ESRL
Ile grande, FR (LPO)	2004-2013	LSCE
Mawson, AU (MAA)	1990-2013	WDCGG/ CSIRO
Mould Bay, Nunavut, CA (MBC)	1980-1997	NOAA/ ESRL
Mace Head, County Galway, IE (MHD)	1991-2013	NOAA/ ESRL
Mace Head, County Galway, IE (MHD)	1996-2013	LSCE
Sand Island, Midway, US (MID)	1985-2013	NOAA/ ESRL
Mt. Kenya, KE (MKN)	2003-2011	NOAA/ ESRL
Mauna Loa, Hawaii, US (MLO)	1979-2013	NOAA/ ESRL
Macquarie Island, AU (MQA)	1990-2013	WDCGG/ CSIRO
Gobabeb, NA (NMB)	1997-2013	NOAA/ ESRL
Niwot Ridge, Colorado, US (NWR)	1979-2013	NOAA/ ESRL
Olympic Peninsula, WA, USA (OPW)	1984-1990	NOAA/ ESRL
Ochsenkopf, DE (OXK)	2003-2013	NOAA/ ESRL
Pallas-Sammaltunturi, GAW Station, FI (PAL)	2001-2013	NOAA/ ESRL

Pic du Midi, FR (PDM)	2001-2013	LSCE
Pacific Ocean, 0N (POC000)	1987-2011	NOAA/ ESRL
Pacific Ocean, 5N (POCN05)	1987-2011	NOAA/ ESRL
Pacific Ocean, 10N (POCN10)	1987-2011	NOAA/ ESRL
Pacific Ocean, 15N (POCN15)	1987-2011	NOAA/ ESRL
Pacific Ocean, 20N (POCN20)	1987-2011	NOAA/ ESRL
Pacific Ocean, 25N (POCN25)	1987-2011	NOAA/ ESRL
Pacific Ocean, 30N (POCN30)	1987-2011	NOAA/ ESRL
Pacific Ocean, 5S (POCS05)	1987-2011	NOAA/ ESRL
Pacific Ocean, 10S (POCS10)	1987-2011	NOAA/ ESRL
Pacific Ocean, 15S (POCS15)	1987-2011	NOAA/ ESRL
Pacific Ocean, 20S (POCS20)	1987-2011	NOAA/ ESRL
Pacific Ocean, 25S (POCS25)	1987-2011	NOAA/ ESRL
Pacific Ocean, 30S (POCS30)	1987-2011	NOAA/ ESRL
Pacific Ocean, 35S (POCS35)	1987-2011	NOAA/ ESRL
Palmer Station, Antarctica, US		
(PSA)	1979-2013	NOAA/ ESRL
Point Arena, California, US (PTA)	1999-2011	NOAA/ ESRL
Puy de Dome, FR (PUY)	2001-2013	LSCE
Ragged Point, BB (RPB)	1987-2013	NOAA/ ESRL
South China Sea, 3N (SCSN03)	1991-1998	NOAA/ ESRL
South China Sea, 6N (SCSN06)	1991-1998	NOAA/ ESRL
South China Sea, 9N (SCSN09)	1991-1998	NOAA/ ESRL
South China Sea, 12N (SCSN12)	1991-1998	NOAA/ ESRL
South China Sea, 15N (SCSN15)	1991-1998	NOAA/ ESRL

South China Sea, 18N (SCSN18)	1991-1998	NOAA/ ESRL
South China Sea, 21N (SCSN21)	1991-1998	NOAA/ ESRL
Mahe Island, SC (SEY)	1980-2013	NOAA/ ESRL
Southern Great Plains, Oklahoma, US (SGP)	2002-2013	NOAA/ ESRL
Shemya Island, Alaska, US (SHM)	1985-2013	NOAA/ ESRL
Ship between Ishigaki Island and Hateruma Island, JP (SIH)	1993-2005	WDCGG/ Tohoku University
Shetland, Scotland, GB (SIS)	1992-2003	WDCGG/ CSIRO
Tutuila, American Samoa (SMO)	1979-2013	NOAA/ ESRL
South Pole, Antarctica, US (SPO)	1979-2013	NOAA/ ESRL
Ocean Station M, NO (STM)	1980-2009	NOAA/ ESRL
Summit, GL (SUM)	1997-2013	NOAA/ ESRL
Syowa Station, Antarctica, JP (SYO)	1986-2013	NOAA/ ESRL
Tae-ahn Peninsula, KR (TAP)	1991-2013	NOAA/ ESRL
Tierra Del Fuego, Ushuaia, AR (TDF)	1994-2013	NOAA/ ESRL
Trinidad Head, California, US (THD)	2002-2013	NOAA/ ESRL
Tromelin Island, F (TRM)	1998-2007	LSCE
Wendover, Utah, US (UTA)	1993-2013	NOAA/ ESRL
Ulaan Uul, MN (UUM)	1992-2013	NOAA/ ESRL

Sede Boker, Negev Desert, IL

(WIS)

1995-2013

NOAA/ ESRL

Sable Island, CA (WSA)

1979-2012

WDCGG/ EC

Mt. Waliguan, CN (WLG)

1990-2013

NOAA/ ESRL

Western Pacific Cruise (WPC)

2004-2013

NOAA/ ESRL

Ny-Alesund, Svalbard, Norway

and Sweden (ZEP)

1994-2013

NOAA/ ESRL

665 **Table 2: Same as Table 1 but for the flask-sampling sites.**

666

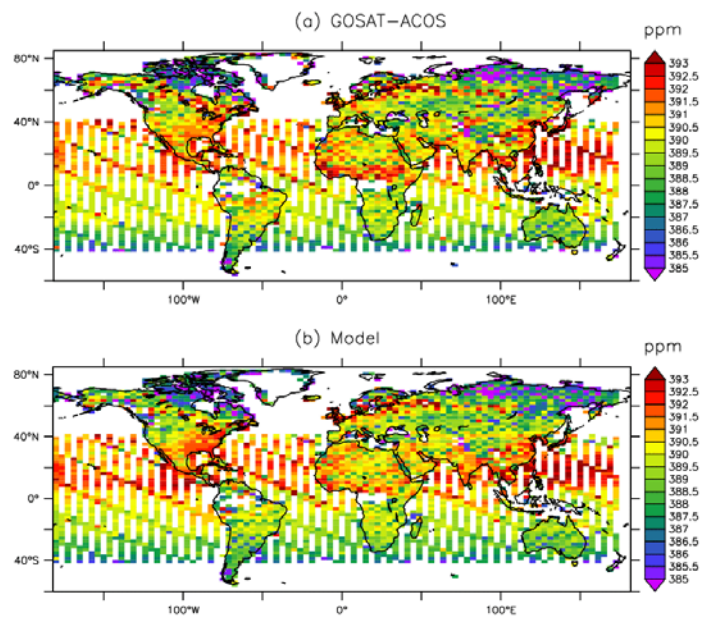
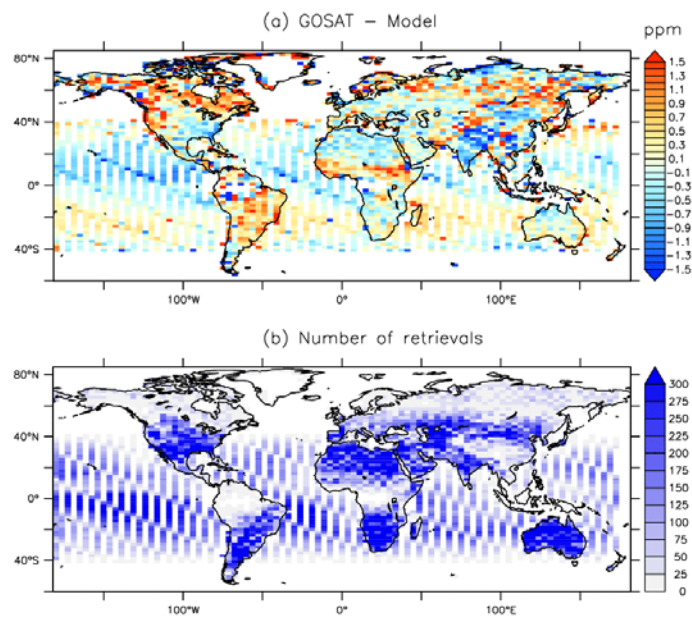


**Fig. 1. (a) Mean ACOS-GOSAT bias-corrected retrievals in the model grid over 4 years (June 2009-May 2013). (b) Corresponding mean CO<sub>2</sub> 4D field associated to the MACC CO<sub>2</sub> inversion (computed using the averaging kernels and the prior profiles of the retrievals).**



672  
 673  
 674 **Fig. 2. (a) Mean difference between the maps of Fig. 1 (retrievals minus model). (b)**  
 675 **Corresponding number of retrievals.**  
 676



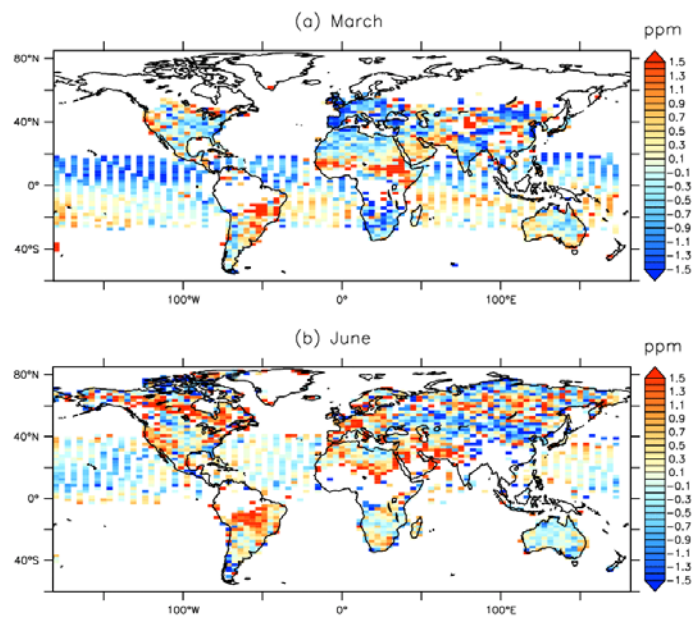
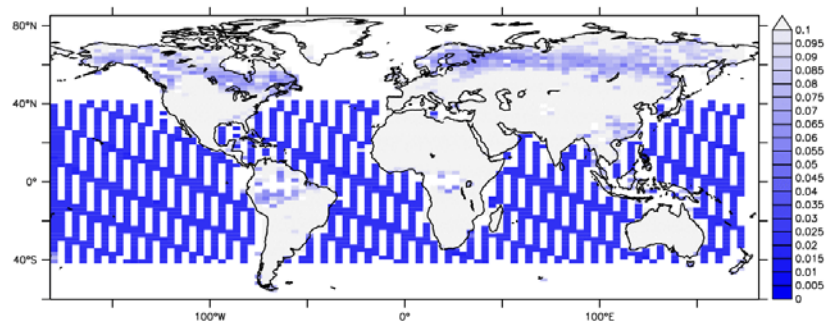


**Fig. 3. Same as Fig. 2(a) (retrievals minus model), but focussing on the months of March and June.**

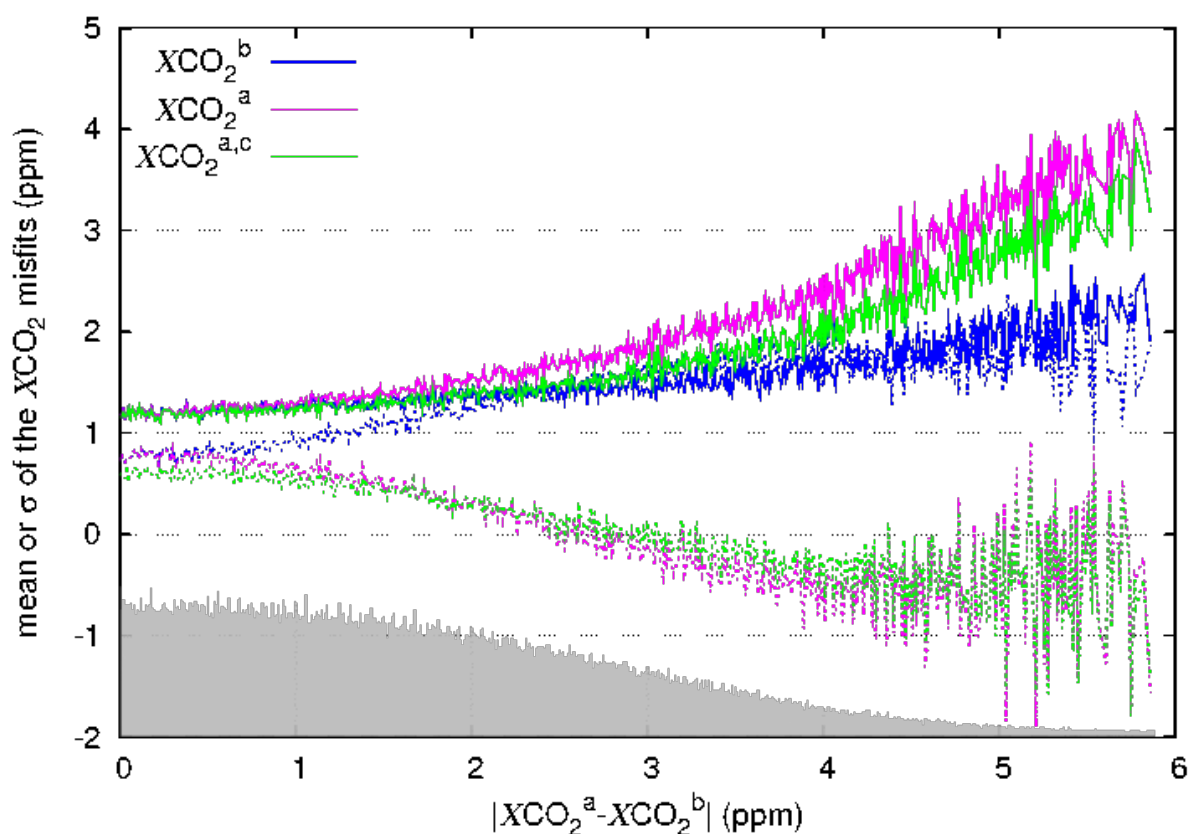


680

681 **Fig. 4. Mean surface albedo retrieved in the strong CO<sub>2</sub> band by ACOS-GOSAT in the**  
 682 **model grid over 4 years (June 2009-May 2013). The blue scale focuses on the values less**  
 683 **than 0.1.**

684

685



686

687 **Fig. 5. Mean and standard deviation of the retrieval-minus-model misfits between June**  
 688 **2009 and May 2013 for the high-gain mode retrievals over land as a function of the retrieval**  
 689 **increment size. The statistics are also shown for the prior-minus-model misfit. The model**  
 690 **values are raw pressure-weighted columns and do not account for the averaging kernels in**  
 691 **order not to correlate the two axes (in practice, using the averaging kernels actually does**  
 692 **not significantly affect the standard deviations shown). The grey shade shows the**  
 693 **distribution of the retrieval density (axis not shown).**

694

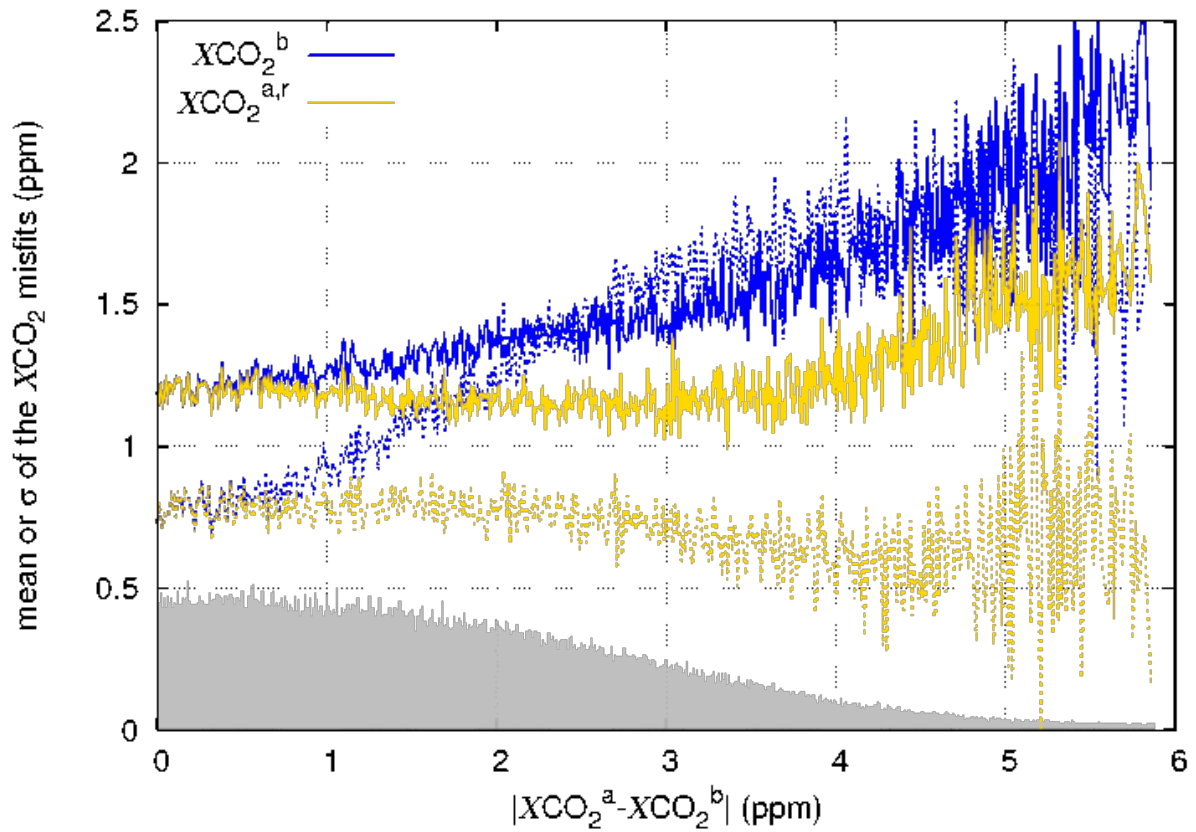
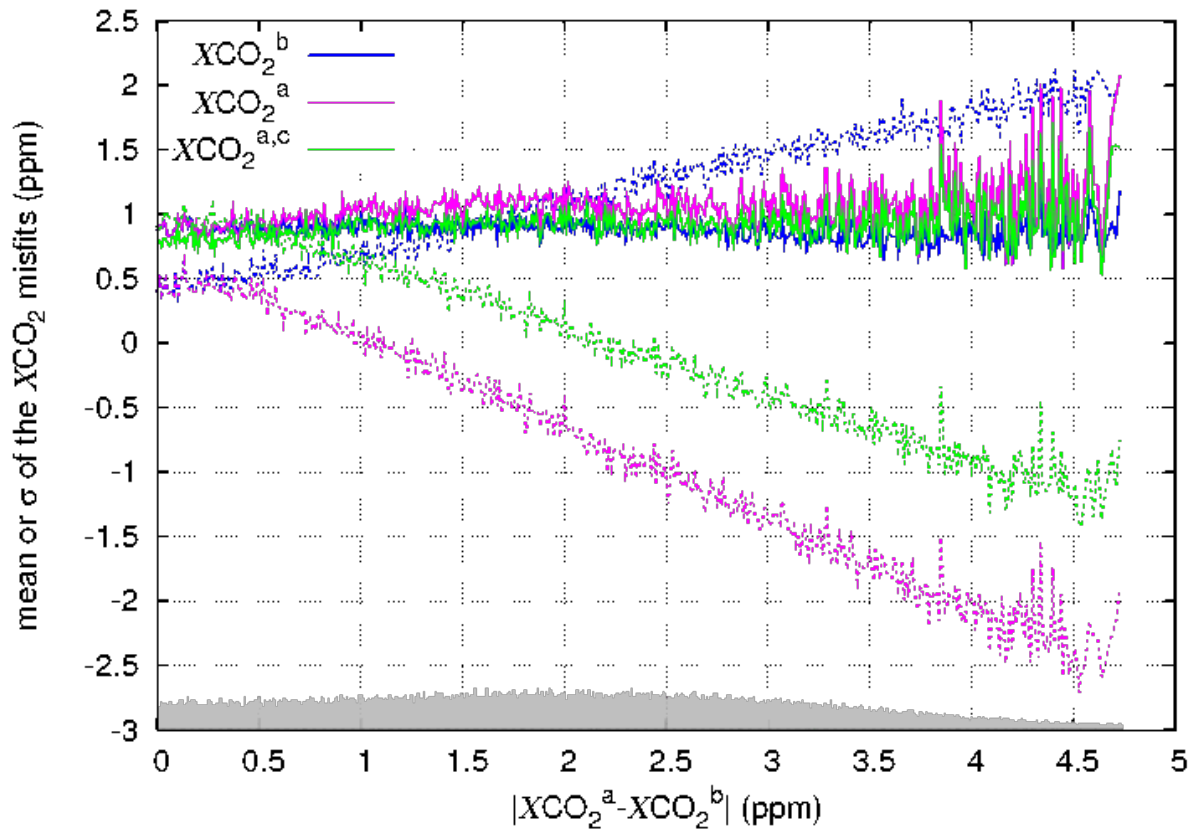


**Fig. 6.** Same as Fig. 5 (high-gain mode over the lands) but we reduce the retrieval increment size by 50% without any bias correction (we call  $XCO_2^{a,r}$  the result). The abscissa shows the unperturbed increment.



701

702 **Fig. 7. Same as Fig. 5 for the medium-gain mode.**

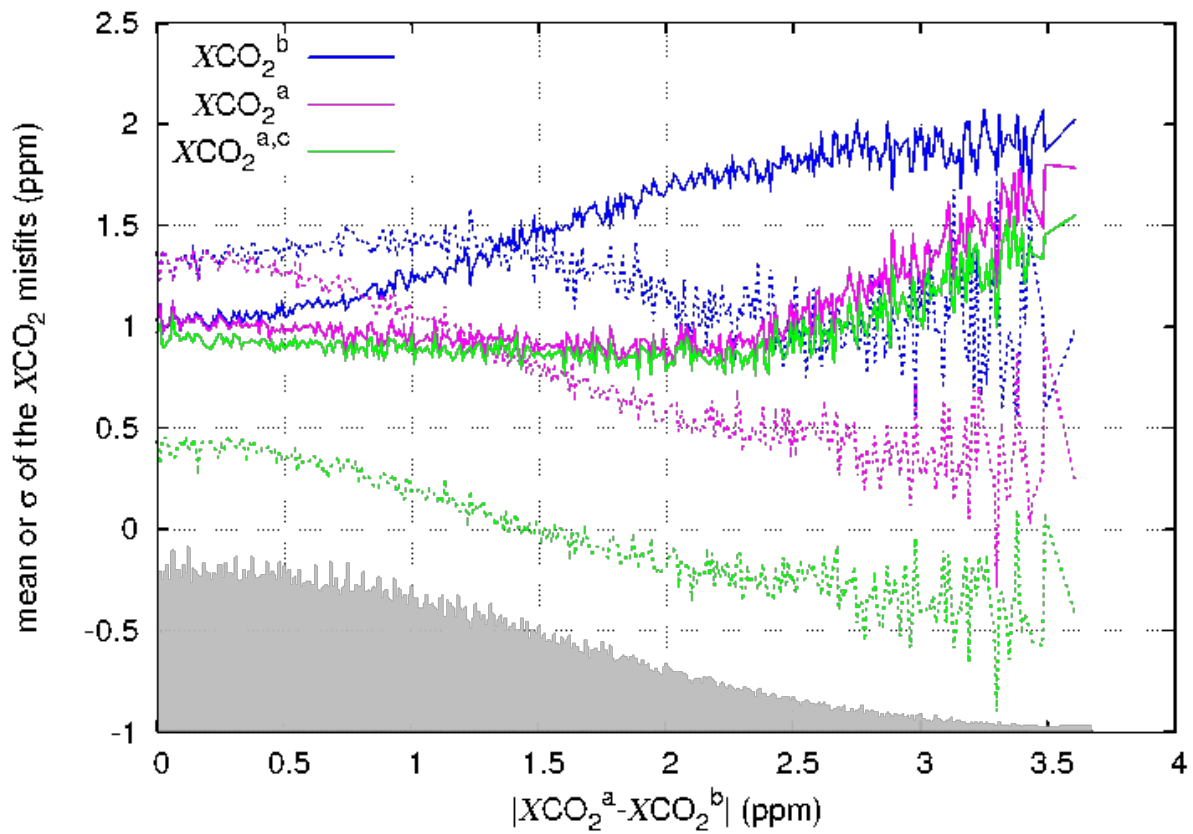


**Fig. 8. Same as Fig. 5 for the glint mode over the ocean.**